ISSN 1063-7834, Physics of the Solid State, 2009, Vol. 51, No. 4, pp. 810–816. © Pleiades Publishing, Ltd., 2009.
Original Russian Text © K.S. Aleksandrov, V.N. Voronov, A.N. Vtyurin, A.S. Krylov, M.S. Molokeev, M.S. Pavlovskiĭ, S.V. Goryaĭnov, A.Yu. Likhacheva, A.I. Ancharov, 2009, published in Fizika Tverdogo Tela, 2009, Vol. 51, No. 4, pp. 764–770.

LATTICE DYNAMICS AND PHASE TRANSITIONS

Pressure-Induced Phase Transition in the Cubic ScF_3 Crystal

K. S. Aleksandrov[a], V. N. Voronov[a], A. N. Vtyurin[a]*, A. S. Krylov[a], M. S. Molokeev[a], M. S. Pavlovskiĭ[a], S. V. Goryaĭnov[b], A. Yu. Likhacheva[b], and A. I. Ancharov[c]

[a] *Kirensky Institute of Physics, Siberian Branch, Russian Academy of Sciences, Akademgorodok, Krasnoyarsk, 660036 Russia*
**e-mail: vtyurin@iph.krasn.ru*

[b] *Institute of Geology and Mineralogy, Siberian Branch, Russian Academy of Sciences, Novosibirsk, 630090 Russia*

[c] *Institute of Solid State Chemistry, Siberian Branch, Russian Academy of Sciences, Novosibirsk, 630091 Russia*

Received June 19, 2008

Abstract—Pressure-induced phase transitions in the ScF_3 crystal were studied using synchrotron radiation diffraction, polarization microscopy, and Raman spectroscopy. The phase existing in the range 0.6–3.0 GPa is optically anisotropic; its structure is described by space group $R3c$ ($Z = 2$), and the transition is due to rotation of ScF_6 octahedra around a threefold axis. The pressure dependence of the structural parameters and angle of rotation are determined. The number of Raman spectral lines corresponds to that expected for this structure; above the phase transition point, a recovery of soft modes takes place. At a pressure of 3.0 GPa, a transition occurs to a new phase, which remains metastable as the pressure decreases. The results are interpreted using an ab initio method based on the Gordon–Kim approach.

PACS numbers: 61.50.Ks, 63.70.+h, 64.70.kp, 78.30.Hv, 81.30.Dz

DOI: 10.1134/S1063783409040295

1. INTRODUCTION

Fluorides of trivalent metals $MeF_3$with the ideal or distorted α-ReO_3 structure belong to the family of perovskite-like compounds with the general formula ABX_3 in which one of the cation sites is vacant (Fig. 1). Like all the perovskites, these crystals undergo sequential phase transformations under external actions. Owing to their simple structure, they are attractive model objects for studying the mechanisms of phase transitions (see, e.g., [1]), and the existence of volume voids in their structure makes it possible to smoothly vary their physical properties by creating a structural disorder or introducing impurities, which opens possibilities of their practical applications [2, 3].

Among the other compounds with the chemical formula MeF_3, scandium fluoride is likely the least understood. There is no information about this compound in the most complete reviews devoted to the description of structural phase transitions in perovskites [4, 5]. The structural data base [6] contains information about three different structures of ScF_3 under normal conditions: cubic, rhombohedral, and orthorhombic. However, special studies of the stability of these phases [7] showed that the orthorhombic phase is metastable under normal conditions, and the cubic phase was not detected at all.

As noted in [5, 8, 9], the phase diagrams of these crystals is very sensitive to structural defects and impurities, which additionally hampers their studies. Moreover, at least some of the phase transitions in the crystals of this family are ferroelastic [1, 4] and the existence of growth stresses in samples synthesized at high temperatures can also substantially influence their behavior as the external conditions vary.

In [10], the vibrational spectra of the ScF_3 cubic lattice were studied at low temperatures down to 4 K and no phase transitions were detected. In [11], ab initio calculations by the Gordon–Kim method predicted that the cubic phase of this crystal must lose its stability under hydrostatic pressure, and indications of this transition were detected by Raman spectroscopy. The aim

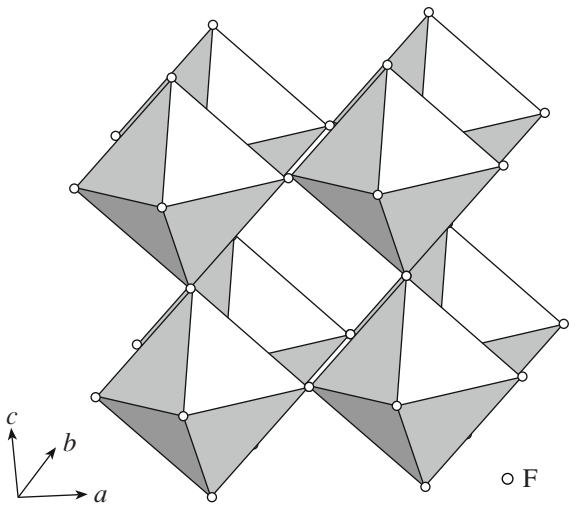

Fig. 1. Structure of the ScF_3 cubic phase (schematic): scandium ions are in the centers of octahedra.

of this work is to study the sequence of phase transitions in the ScF_3 crystal under pressure and the structure of the high-pressure phase using synchrotron radiation diffraction, Raman spectroscopy, and polarization microscopy and to elucidate the nature of the lattice instability using nonempirical calculations in terms of a microscopic model of ionic crystal.

2. EXPERIMENTAL

We studied the same ScF_3 single crystals as in [11], which were grown from solution in a melt of lithium fluoride; the growth method is described in detail in [11]. Observations with a polarization microscope showed that the samples are optically isotropic (which agrees with the cubic structure of the normal-pressure phase) and do not contain visible defects and inclusions. X-ray diffraction analysis showed that their structure corresponds to the cubic phase of ScF_3 with a unit-cell parameter $a_0 = 4.01$ Å (the comparison was carried out using the data from [6]).

The room-temperature experiments under high hydrostatic pressure (up to 8 GPa) were performed on a setup with diamond anvils similar to that used in [12, 13]. The chamber with a sample was 0.25 mm in diameter and 0.1 mm in height. The pressure was determined to within 0.05 GPa from the shift of the luminescence band of a ruby microcrystal [13, 14] placed near the sample. As a pressure-transmitting medium, we used carefully dehydrated mixtures of ethyl and methyl alcohols, dehydrated glycerin, or (at small pressures not causing crystallization) doubly distillated water. All the experimental results show that there is no dependence on the type of pressure-transmitting medium.

The X-ray diffraction patterns of the polycrystalline ScF_3 sample were obtained at room temperature at pressures of 1.38, 2.10, 2.62, and 3.25 GPa, corresponding to the region of existence of the first high-pressure phase according to [11], on an X-ray powder diffractometer using synchrotron radiation (λ = 0.36750 Å) and a MAR3450 two-coordinate detector (VÉPP-3 accelerator) at the Institute of Nuclear Physics (Siberian Branch, RAS, Novosibirsk). The high-pressure cell was placed on a goniometric head in such a manner that a foil with the sample was perpendicular to the beam, and thereafter it was centered. The collimator of an X-ray beam was 0.1 mm in diameter; so, the foil was not struck by the beam and did not give an undesirable background. However, all the diffraction patterns show bright spots corresponding to reflections of a diamond single crystal. These spots were removed using special markers in the Fit2D program [15], which excluded the appearance of excess peaks in a Debye powder pattern. The determination of the centers of rings and the integration of the Debye powder pattern were also performed using the Fit2D program. The angle 2θ was varied in the X-ray diffraction pattern in steps of 0.01°. With the integrated Debye powder patterns, the unit-cell parameters of the crystal were determined using the WTREOR program [16]. The search for crystal structures was carried out using the FOX program [17], and the structural parameters were refined by the full-profile Rietveld method using the WINPLOTR program [18].

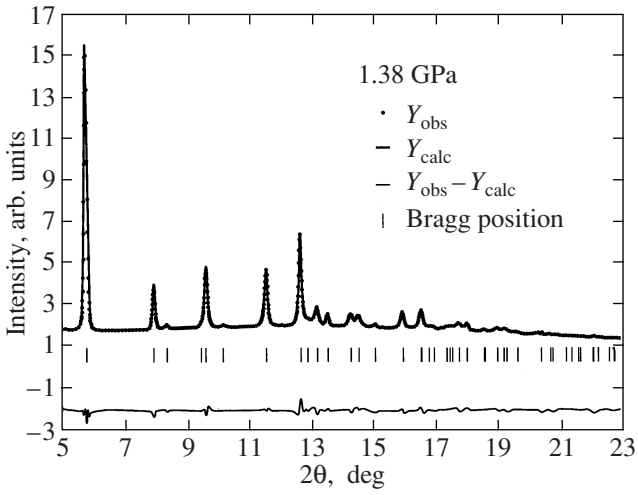

Fig. 2. Debye X-ray powder pattern of the ScF_3 rhombohedral phase at a pressure of 1.38 GPa.

The Raman spectra were recorded using a T64000 (Horiba–Jobin Yvon) triple-crystal spectrometer in the micro-Raman configuration with matrix recording in backscattering geometry (resolution 0.3 cm^{-1} per pixel). Because of the presence of a strong wing of elastic scattering, on which the spectrum of air scattering is superposed, the spectrum was recorded over the range 100–600 cm^{-1}. The spectrum was excited by an Ar-laser line (Spectra Physics 2017, 514.5 nm, 100 mW). Simultaneously, birefringence was studied. To obtain quantitative information about the parameters of the spectral lines, the data were processed by the PeakFit (SeaSolve Software Inc.) program package using the Voigt profile to fit individual lines.

3. THE STRUCTURE OF THE HIGH-PRESSURE PHASE

The typical Debye powder pattern and the results of its processing are shown in Fig. 2. For all pressures studied, the extinctions correspond to space groups $R3c$ or $R\bar{3}c$. The structure with space group $R3c$ (Fig. 3) best describes the experimental X-ray diffraction pattern and is chosen for further refinement. The main parameters of the data acquisition and the results of refining the structural parameters are presented in Table 1.

When searching for the structure, two independent atoms corresponding to Sc and F atoms are found in the independent portion of the unit cell. To describe the peak shapes, we chose Pirson function VII at 6.0 FWHM for refinement of the profile and 20.0 FWHM

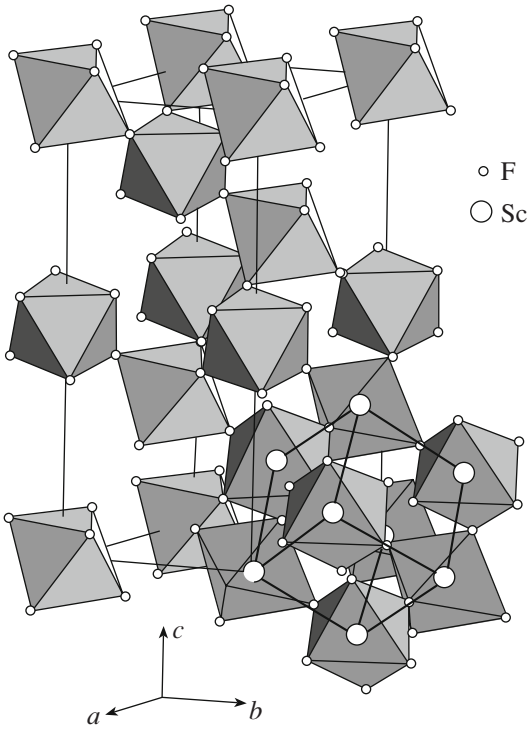

Fig. 3. Structure of the ScF_3 rhombohedral phase. At the bottom right, the unit cell of the cubic phase is shown.

for final refinement of the structure, where FWHM is the average peak full width at half-maximum. The first stage of refining both the structures was fitting of the profile peaks performed in several steps. First, we refined the unit-cell parameters, the shift of the counter zero, and the first coefficient of the polynomial describing the background. Then, we successively added the profile parameters *U*, *V*, *W*, *X*, and *Y* and other coefficients of the polynomial. The profile refinement was ended by a correction of the peak asymmetry parameters. The second step was the refinement of the structure. The coordinate of an F atom and isotropic thermal parameters of both the atoms were only refined. Then, we made a correction for a possible predominant orientation of the powder grains. As a model, the exponential function $P_h = G_2 + (1 - G_2)\exp(G_1\alpha_h^2)$ was chosen, where G_1 and G_2 are adjustable parameters and α_h is the angle between the scattering vector and a given direction of the predominant orientation of the grains in reciprocal space, which is chosen experimentally. In our case, the 001 orientation leads to minimum *R* factors for all the X-ray diffraction patterns. The results of the refinement of the structures are given in Table 2.

An analysis of the high-pressure phases shows that, during the phase transition, the ScF_6 octahedron rotates around a threefold axis and remains almost undistorted. The Sc–F bond lengths are within the range 1.9–2.1 Å, which agrees with a typical Sc–F bond length of 2.075 Å for the octahedral surroundings of the Sc ion consisting of F ions.

4. VARIATIONS OF THE RAMAN SPECTRA

The vibrational representation of space group *Pm*3*m* of the cubic phase at the Brillouin zone center has the form

$$\Gamma_0 = F_{2u} + 3F_{1u}, \quad (1)$$

where all vibrational modes are Raman inactive.

The analogous expansion for the rhombohedral structure is

$$\Gamma_1 = \mathbf{A_{1g}} + 2A_{2g} + \mathbf{3E_g} + 2A_{1u} + 3A_{2u} + 5E_u, \quad (2)$$

and, for the orthorhombic structure,

$$\Gamma_2 = \mathbf{7A_g} + \mathbf{5B_{1g}} + \mathbf{7B_{2g}} + \mathbf{5B_{3g}} + 5A_u + 7B_{1u} + 5B_{2u} + 7B_{3u}. \quad (3)$$

In Eqs. (2) and (3), Raman-active modes are in boldface.

Table 1. Parameters of the data acquisition and the results of refinement of the structure of the first ScF_3 high-pressure phase

Parameter	Pressure, GPa			
	1.38	2.1	2.62	3.25
Space group	*R*3*c*	*R*3*c*	*R*3*c*	*R*3*c*
a, Å	5.30874(4)	5.24434(6)	5.07838(8)	5.04489(3)
c, Å	14.070555(4)	14.109255(7)	14.278027(7)	14.260591(3)
V, Å^3	343.421(2)	336.060(3)	318.896(4)	314.320(2)
Range of 2θ angles, deg	5–23	5–20	5–23	5–20
Number of Bragg reflections	53	35	51	33
Number of refined parameters	10	10	10	10
R_{wp}, %	13.4	12.1	16.7	8.27
R_B, %	5.95	13.4	9.76	6.40

As is seen from comparing Eqs. (1)–(3), the selection rules for these structures differ substantially and they can be easily identified using the Raman spectra.

At normal pressure, there is no Raman spectrum in the crystal; the crystal is optically isotropic and reveals good extinction between crossed polarizers (a slight blooming occurs owing to anisotropic mechanical stresses in the diamond anvils). At a pressure of 0.6 GPa, two weak lines arise in the spectrum (at 263 and 437 cm^{-1}, Fig. 4); simultaneously, blooming of the sample between crossed polarizers occurs, which indicates that the crystal becomes optically anisotropic. In some samples, a partition into large domains (of the order of 0.02–0.05 mm) of irregular shape is observed. As the pressure is increased further, the intensity of these lines increases monotonically and the frequency of the line at 263 cm^{-1} increases to 303 cm^{-1} at 3.0 GPa. One more line appears in the low-frequency range (at 144 cm^{-1} at 1.1 GPa). At 1.8 GPa, it is split into a doublet, whose components are monotonically shifted to 200 and 243 cm^{-1} at 3.0 GPa. Note that, at each change in pressure, the exciting radiation is focused anew; so, the proportion of the intensities of the doublet components cannot be correctly measured. However, the fact that this proportion changes substantially with a change in the alignment may be indicative of different polarizations of these lines. The pressure dependences of the frequencies of the observed lines are shown in Fig. 5.

Simultaneously, as the pressure increases, the birefringence of the sample is enhanced and the interferential color of the sample is changed owing to a change in the shape of the optical indicatrix.

The changes occurring up to 3.0 GPa are reversible and are reproduced for different samples of the same crystallization and for different pressure-transmitting liquids. Hysteresis phenomena are not observed to within the accuracy of measurements. The domain structure, which is largely determined by defects at the sample boundaries, is changed from sample to sample and depends on the rate of pressure change. We succeed in obtaining a single-domain state in well-faceted microcrystals when the pressure was increased slowly.

When the pressure is increased further above 3.0 GPa, one more transition occurs. A complex system of numerous small (smaller than 0.01 mm) domains visible through a microscope arises in the crystal; the domain boundaries strongly scatter the light. Simultaneously, the Raman spectrum is varied sharply; numerous new separate lines and bands appear, which are likely to consist of several close-spaced profiles (Figs. 4, 5). Note that the transition point 3.0 GPa agrees well with the transition pressure from the rhombohedral to the orthorhombic phase of this crystal observed in [8, 9]. As the pressure increases further, the Raman spectrum is changed only slightly; namely, only the shift and splitting of the components of the low-frequency doublet that appeared during the previous transition increase in value.

Table 2. Coordinates of atoms and isotropic thermal parameters of ScF_3 at various pressures

Atom	Position population	x	y	z	B_{iso}, Å^2
		P = 1.38 GPa			
Sc	1.0	0	0	0	1.28(9)
F	1.0	0.256(1)	0.314(3)	0.0892(8)	0.8(1)
		P = 2.10 GPa			
Sc	1.0	0	0	0	1.77(9)
F	1.0	0.284(5)	–0.075(3)	0.090(3)	1.2(1)
		P = 2.62 GPa			
Sc	1.0	0	0	0	0.5
F	1.0	0.303(2)	0.282(1)	–0.0926(7)	0.5
		P = 3.25 GPa			
Sc	1.0	0	0	0	1.17(5)
F	1.0	0.304(2)	–0.041(2)	0.080(1)	0.55(7)

The system of domain boundaries formed on the transition is slightly modified as the pressure increases; the total number of the domains decreases somewhat, but the system does not disappear completely. The crystal remains optically anisotropic, although the strong scattering by the domain walls hampers the observation of the related effects.

A decrease in pressure in this phase does not cause a reverse transition. The system of domain boundaries and the general character of the Raman spectrum remain. When the pressure is decreased slowly (for several hours) from 1 GPa, the sample survives down to normal pressure (as noted in [11], the abrupt removal of pressure damages the sample). This metastable high-pressure phase is retained irrespective of the type of pressure-transmitting liquid used. Holding of the sample under pressure at a high temperature (150°C) for 1 h also did not cause any changes.

5. DISCUSSION OF THE RESULTS

To analyze the effect of pressure on the structure and vibration spectrum of the ScF_3 crystal lattice, we used a nonempirical model of ionic crystal that generalizes the Gordon–Kim approximation by taking into account the influence of the crystal lattice on the deformability and polarizability of the ions [19, 20]. In terms of this model, the lattice dynamics of the ScF_3 cubic phase and isomorphic crystals, such as AlF_3, GaF_3, and InF_3, were simulated in [11]. The vibration spectrum of the ScF_3 lattice in the cubic phase calculated in [11] does not contain imaginary frequencies (which explains the stability of the structure down to 4 K); however, it has a weakly dispersed branch (between points R and M of the Brillouin zone) with an anomalously low frequency.

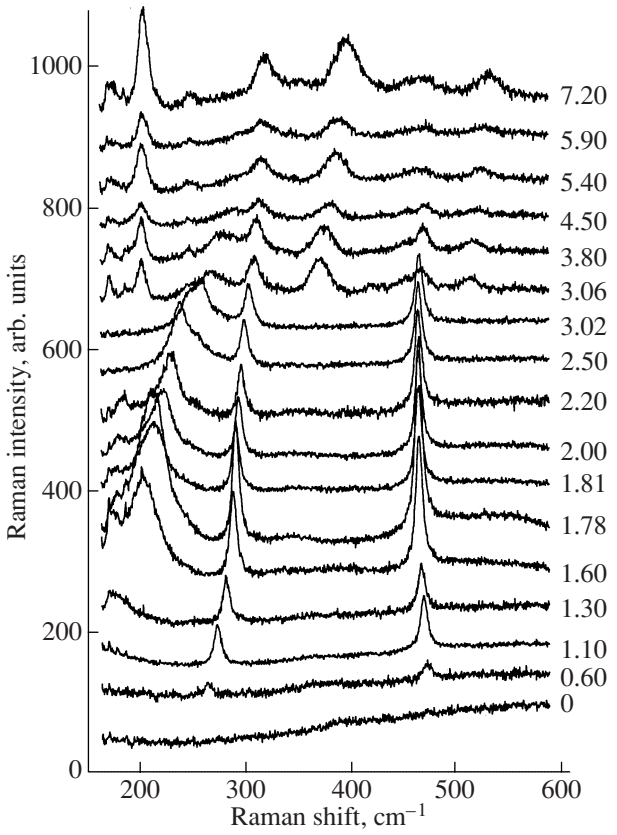

Fig. 4. Transformation of the Raman spectrum with increasing pressure (indicated in gigapascals near the curves).

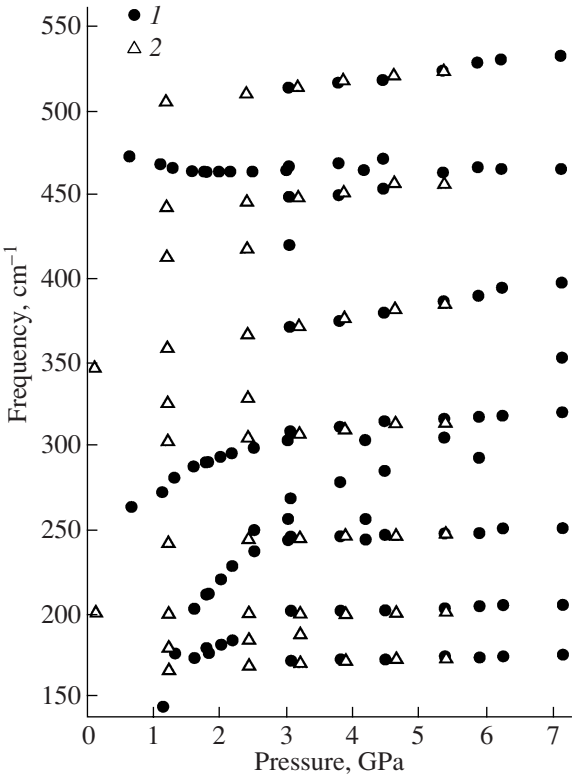

Fig. 5. Pressure dependence of the frequencies of the Raman spectral lines: (*1*) compression and (*2*) decrease in pressure from the second high-pressure phase.

In this vibration branch, triply degenerate mode R_5 at point R and nondegenerate modes on the $R \longrightarrow M$ line (including point M) involve fluorine ions [20]. It is the condensation of modes of this vibration branch that causes structural phase transitions in most halides with a perovskite structure [4], among them MeF_3 crystals (Me = Al, Ga, In, etc.) [1, 2].

In order to analyze the effect of pressure on the stability and vibration spectrum of the ScF_3 lattice, an analogous calculation was performed for decreasing unit-cell parameters. The correlation between the pressure and the unit-cell parameter was estimated by numerically differentiating the total energy of the crystal with respect to its volume and using the bulk modulus $B = (C_{11} + 2C_{12})/3$ determined from the elastic constants calculated in [11].

The most substantial changes in the calculated lattice vibration spectrum of the cubic phase with an increase in hydrostatic pressure occur at low and high frequencies of the optical vibrational modes. As the volume decreases, the high-frequency vibrational modes become harder. On the contrary, the lattice vibration branch between points R and M of the Brillouin zone with anomalously low frequencies becomes softer with increasing pressure, which causes instability of the cubic crystal lattice. The reason for this is that short-range ion–ion interactions (for the most part, dipole–dipole interactions of the chlorine ions) increase rapidly and, as a result, their balance with long-range Coulomb interactions is disturbed [11]. The softest mode is the triply degenerate mode R_5 at the boundary point $R = (\pi/a)(1, 1, 1)$ of the Brillouin zone of the cubic phase. It is likely that the phase transition occurring at 0.6 GPa is due to the condensation of this mode.

The displacements of the fluorine ions in the triply degenerate mode R_5 correspond to rotation of the ScF_6 octahedron [20, 21] around a threefold axis of the cubic unit cell. The structural distortions caused by the condensation of this mode and stabilizing the lattice correspond to the experimentally detected structure of the first high-pressure phase (Fig. 3). Figure 6 shows the dependence of the total energy of the crystal with double unit cell at a pressure $P = 6$ GPa on the shifts of the fluorine ions from their equilibrium positions in the cubic phase

$$\tilde{u}^x_{F_1} = -\tilde{u}^y_{F_1} = \tilde{u}^y_{F_2} = -\tilde{u}^z_{F_2} = -\tilde{u}^x_{F_3} = \tilde{u}^z_{F_3} = u, \quad (4)$$

$$\tilde{u}^\alpha_{F_i} = \frac{u^\alpha_{F_i}}{2a}\exp(i\mathbf{q}_R\mathbf{r}), \quad (5)$$

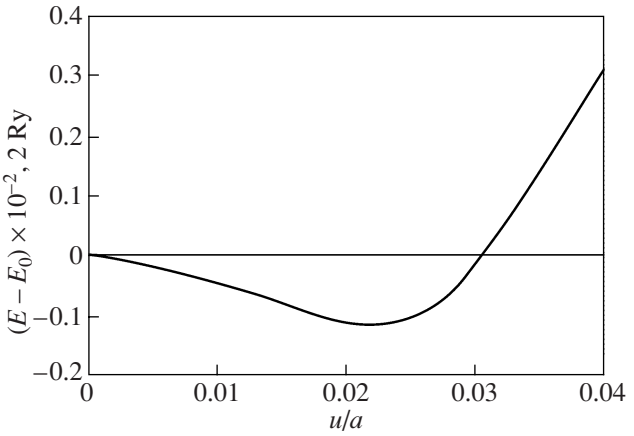

Fig. 6. Dependence of the total energy of the crystal with a doubled unit cell on the fluorine-ion displacement from the equilibrium sites in the cubic phase: $E_0 = -2148.9854$ (in units of 2 Ry) is the total energy of the undistorted phase.

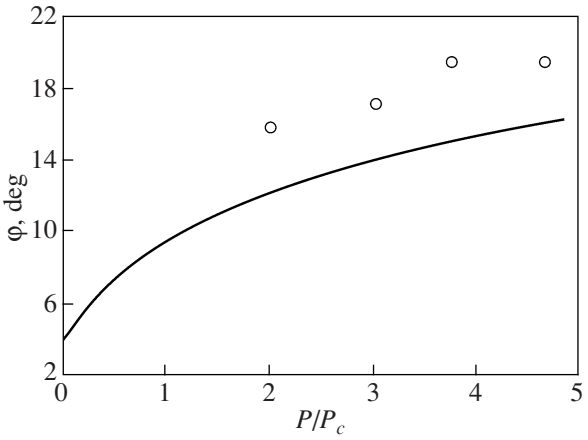

Fig. 7. Calculated (curve) and experimental (points) pressure dependences of the rotation angle of the ScF_6 octahedron in the ScF_3 rhombohedral phase.

where a is the unit-cell parameter of the cubic phase, $\mathbf{r} = m_1\mathbf{a}_1 + m_2\mathbf{a}_2 + m_3\mathbf{a}_3$ is a translation vector, and $\mathbf{q}_R = (\pi/a)(1, 1, 1)$. It is seen that the total energy reaches a minimum at a fluorine-ion shift $u \approx 0.025a$ (0.7 Å). From such calculations, one can obtain the pressure dependence of the structural parameters of the rhombohedral phase. Figure 7 presents the calculated pressure dependence of the angle of rotation of the octahedron around a threefold axis and also the experimental values obtained using the data from Table 2. It is seen that these dependences are qualitatively similar, although the calculation gives underestimated values of the crystal-lattice deformation.

As might be expected from Eq. (2), four vibration modes become Raman active in the rhombohedral phase. Table 3 shows their frequencies far from the transition point and also the frequencies of these modes calculated using the same approach as in [11, 20] and, for comparison, the frequencies of the corresponding modes in the cubic phase calculated in [11]. There is agreement between the calculated and experimental values. The calculation gives somewhat underestimated values of the frequencies, which can be explained by smaller calculated distortions of the lattice as compared to those observed in experiment. Note that the positions of the spectral lines also correlate well with the frequencies of the Raman spectra of the rhombohedral phases of fluorides of a number of other trivalent metals [22]. On the whole, the Raman spectrum of the first high-pressure phase confirms that it is rhombohedral with space group $R3c$ and $Z = 2$.

Table 3. Frequencies of the Raman-active vibration modes of the ScF_3 rhombohedral phase (in cm^{-1})

Vibration symmetry	Experiment	Calculation	Cubic phase
E_g	180	82	65i (R_5)
E_g	300	225	188 (R_4)
E_g	460	398	445 (R_3)
A_{1g}	240	148	65i (R_5)

The second transition point 3.0 GPa agrees well with the transition from the rhombohedral to orthorhombic phase (space group D_{2h}^{16}, $Z = 4$) observed in [9]. This conclusion also agrees with the sharp increase in the number of lines in the Raman spectrum given by Eq. (3). It was noted in [9] that there is strong diffuse X-ray scattering above the this transition point; the scattering decreases gradually as the pressure is increased. This fact correlates well with the formation of a developed system of domain walls observed through a microscope and with an increase in the domain sizes with pressure. The data from [9] also agree well with the fact that this transition is a pronounced first-order transition and that very large hysteresis is observed with decreasing pressure.

6. CONCLUSIONS

In this work, we have performed experimental studies and numerical calculations of the structure and lattice dynamics of the ScF_3 crystal under hydrostatic pressure.

The structure of the rhombohedral phase detected experimentally at pressures above 0.6 GPa by X-ray diffraction and Raman spectroscopy agrees with the results of nonempirical calculations. The transition occurring under hydrostatic pressure is the result of disturbance of the balance between short-range dipole–dipole and long-range Coulomb interactions of ions and is related to rotation of the ScF_6 octahedra around a threefold axis. Above the transition point, the Raman spectrum shows the recovery of two soft phonon modes.

The pressure and general character of another phase transition (presumably from the rhombohedral to orthorhombic phase) observed at 3.0 GPa agree with those observed in [9]. This transition is a pronounced first-order transition and is accompanied by significant hysteresis effects. The formation of a complex system of domain walls is likely the reason of strong diffuse X-ray scattering in this phase observed in [9].

ACKNOWLEDGMENTS

The authors are grateful to V.I. Zinenko for helpful discussion of the results.

This work was conducted in the framework of Integration Project (no. 3.7) of the Russian Academy of Sciences (Siberian Branch).

REFERENCES

1. Ph. Daniel, A. Bulou, M. Rousseau, J. Nouet, J. L. Fourquet, M. Leblanc, and R. Burriel, J. Phys.: Condens. Matter **2**, 5663 (1990).
2. K. Rotereau, Ph. Daniel, and J. Y. Gesland, J. Phys. Chem. Solids **59**, 969 (1998).
3. K. Rotereau, Ph. Daniel, A. Desert, and J. Y. Gesland, J. Phys.: Condens. Matter **10**, 1431 (1998).
4. K. S. Aleksandrov, A. T. Anistratov, B. V. Beznosikov, and N. V. Fedoseeva, *Phase Transitions in Crystals of the Halide Compounds ABX_3* (Nauka, Novosibirsk, 1981) [in Russian].
5. D. Babel and A. Tressaud, in *Inorganic Solid Fluorides*, Ed. by P. Hagenmuller (Academic, London, 1985), p. 77.
6. *Powder Diffraction Data*, Nos. 75-0877, 46-1243, 44-1096, 43-1145, 32-0989, 17-0836 (International Center for Diffraction Data, Newtown Square, PA, United States, 1999).
7. M. M. Aleksandrova, N. A. Bendeliani, V. D. Blank, and T. I. Dyuzheva, Izv. Akad. Nauk SSSR, Neorg. Mater. **26**, 1028 (1990).
8. V. I. Zinenko and N. G. Zamkova, Fiz. Tverd. Tela (St. Petersburg) **42** (7), 1310 (2000) [Phys. Solid State **42** (7), 1348 (2000)].
9. N. A. Bendeliani, É. Ya. Atabaeva, and V. M. Agotkov, Izv. Akad. Nauk SSSR, Neorg. Mater. **19**, 816 (1983).
10. K. S. Aleksandrov, V. N. Voronov, A. Bulou, A. Robert, P. Daniel, and B. Hennion, in *Abstracts of Papers of the Sixth Japan CIS Symposium on Ferroelectricity, Noda, Japan, 1998* (Noda, 1998), p. 152.
11. K. S. Aleksandrov, V. N. Voronov, A. N. Vtyurin, S. V. Goryainov, N. G. Zamkova, V. I. Zinenko, and A. S. Krylov, Zh. Éksp. Teor. Fiz. **121** (5), 1139 (2002) [JETP **94** (5), 977 (2002)].
12. Q. Wang, G. Ripault, and A. Bulou, Phase Transitions **53**, 1 (1995).
13. S. V. Goryainov and I. A. Belitsky, Phys. Chem. Miner. **22**, 443 (1995).
14. R. G. Munro, G. J. Piermarini, S. Block, and W. B. Holzapfel, J. Appl. Phys. **57**, 165 (1985).
15. A. P. Hammersley, *FIT2D: An Introduction and Overview* (The European Synchrotron Radiation Facility Internal Report, No. ESRF97HA02T, 1997).
16. P.-E. Werner, L. Eriksson, and M. Westdahl, J. Appl. Crystallogr. **18**, 367 (1985).
17. V. Favre-Nicolin and R. Cerný, J. Appl. Crystallogr. **35**, 734 (2002).
18. T. Roisnel and J. Rodrigues-Carvajal, in *Proceedings of the Seventh European Powder Diffraction Conference (EPDIC-7), Barcelona, Spain, 2000* (Mater. Sci. Forum **378–381**, 118 (2001)).
19. O. V. Ivanov and E. G. Maksimov, Zh. Éksp. Teor. Fiz. **108** (5), 1841 (1995) [JETP **81** (5), 1008 (1995)].
20. V. I. Zinenko, N. G. Zamkova, and S. N. Sofronova, Zh. Éksp. Teor. Fiz. **111** (5), 1742 (1998) [JETP **87** (5), 944 (1998)].
21. R. Cowley, Phys. Rev. **134**, 981 (1964).
22. P. Daniel, A. Bulou, M. Rossieau, J. Nouet, and M. Leblanc, Phys. Rev. B: Condens. Matter **42**, 10545 (1990).

Translated by Yu. Ryzhkov